Electronic Supplementary Material (ESI) for Dalton Transactions.

Reversible mechanochoromic studies on AIE-inspired Smart materials and applications on sensing

Huijun Li*, Yanan Wang, Zhouqing Xu*

Department of Chemistry and Chemical Engineering, Henan Polytechnic University, Jiaozuo, Henan 454000, China, lihuijunxgy@hpu.edu.cn; zhqxu@hpu.edu.cn.

Materials Characterization Section

Table S1. Crystal data for **HPU-21.**

Complex	**HPU-21**
Formula	$C_{80}H_{87}N_5O_{26}Zn_4$
formula weight, fw	1796.02
Temperature, *T* [K]	173.00
crystal system	*triclinic*
space group	*P-1*
a [Å]	15.4741(12)
b [Å]	15.5050(12)
c [Å]	18.4963(15)
α [°]	68.944(4)
β [°]	82.918(4)
γ [°]	75.554(4)
V [Å^3]	4007.7(6)
Z	2
ρ [g cm^{-3}]	1.488
μ [mm^{-1}]	1.345
θ range	2.228-52.982
F(000)	1860
goodness-of-fit, GOF	1.037
R_1[a] [I > 2σ (I)]	0.0784
wR_2[b] (all data)	0.2348

[a]$R_1 = \big|\,|F_o| - |F_c|\,\big| / |F_o|$. [b]$wR_2 = [w(|F_o^2| - |F_c^2|)^2 / w|F_o^2|^2]^{1/2}$.

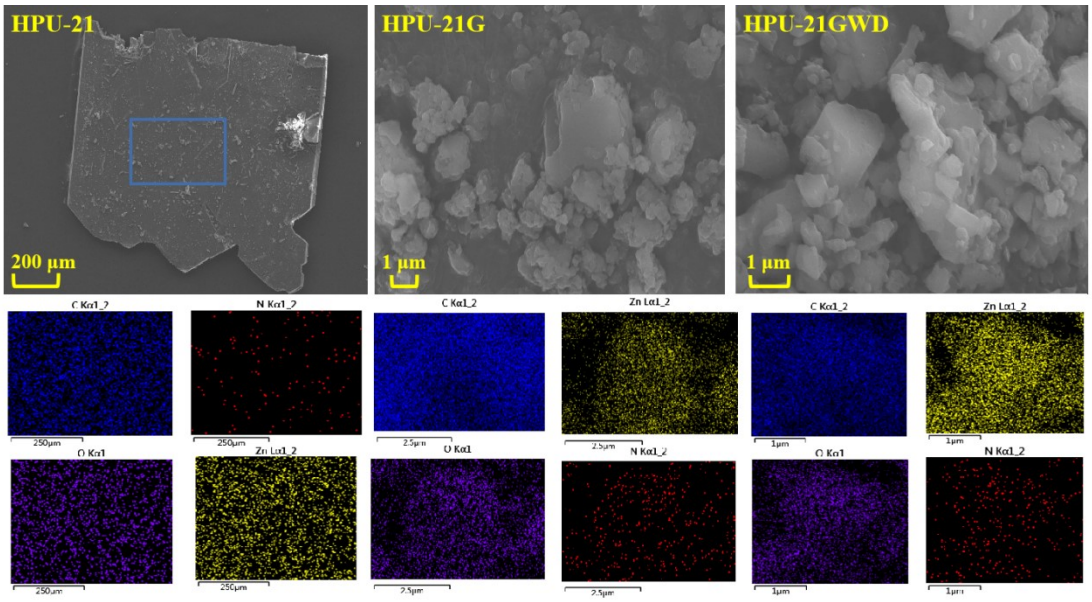

Figure S1. SEM images of cross-sectional morphology of **HPU-21** crystal sample, **HPU-21G** and **HPU-21GWD** disk-like micro/nanosheets obtained.

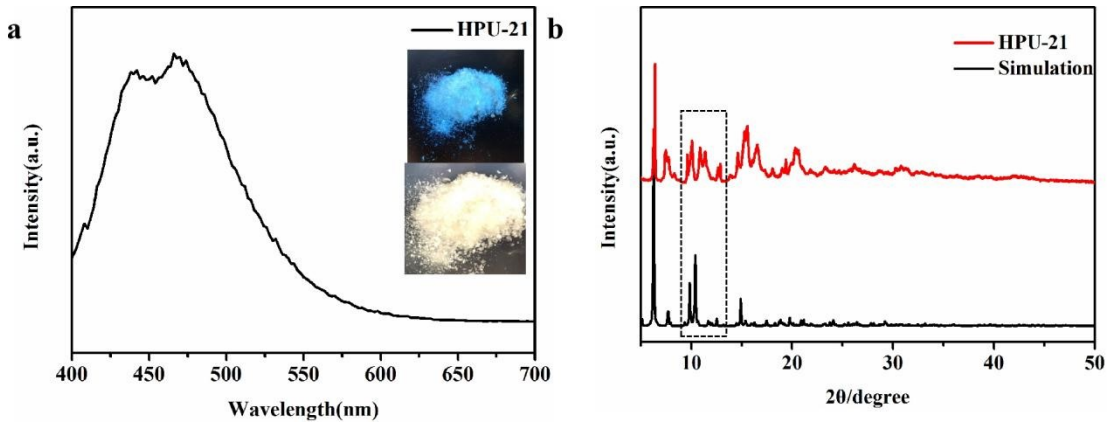

Figure S2. **a**) The emission spectrum of **HPU-21** (Inset is the picture of the crystal under sunlight and ultraviolet light); **b**) The XRD spectrum of the synthesized and the simulated **HPU-21**.

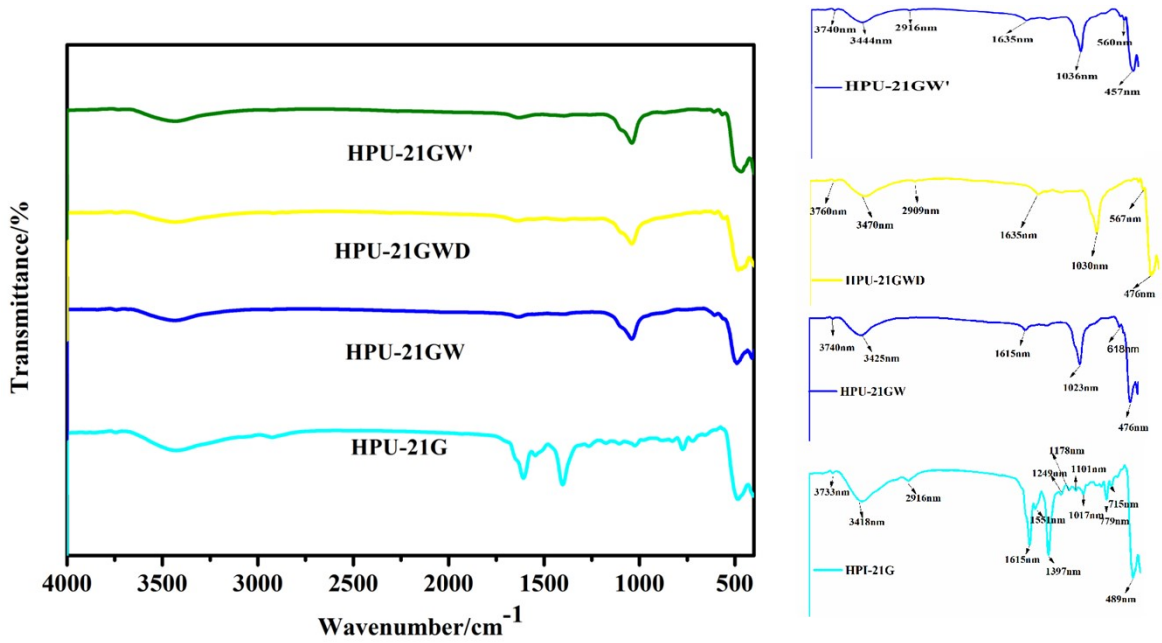

Figure S3. In-situ infrared spectra of **HPU-21G**, **HPU-21GW**, **HPU-21GWD**, and **HPU-21GW'**.

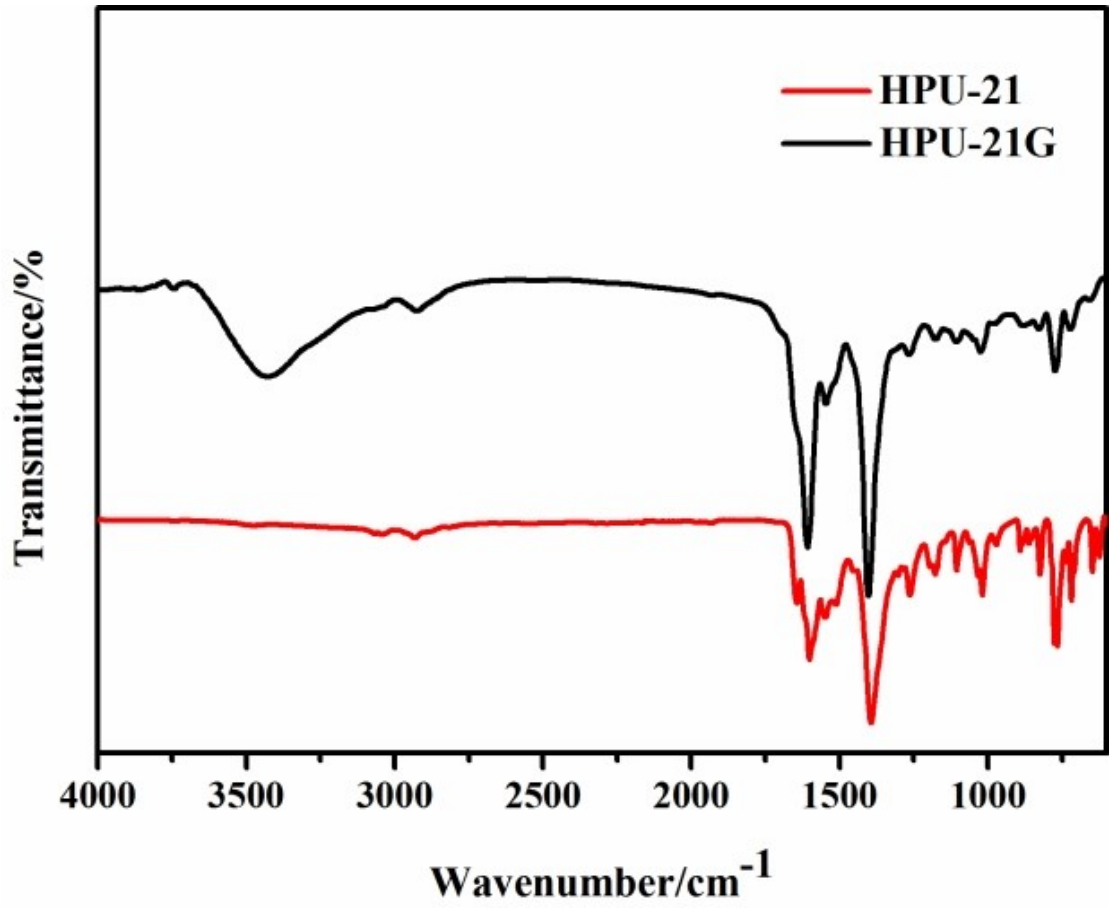

Figure S4. Infrared spectra of **HPU-21** and **HPU-21G**.

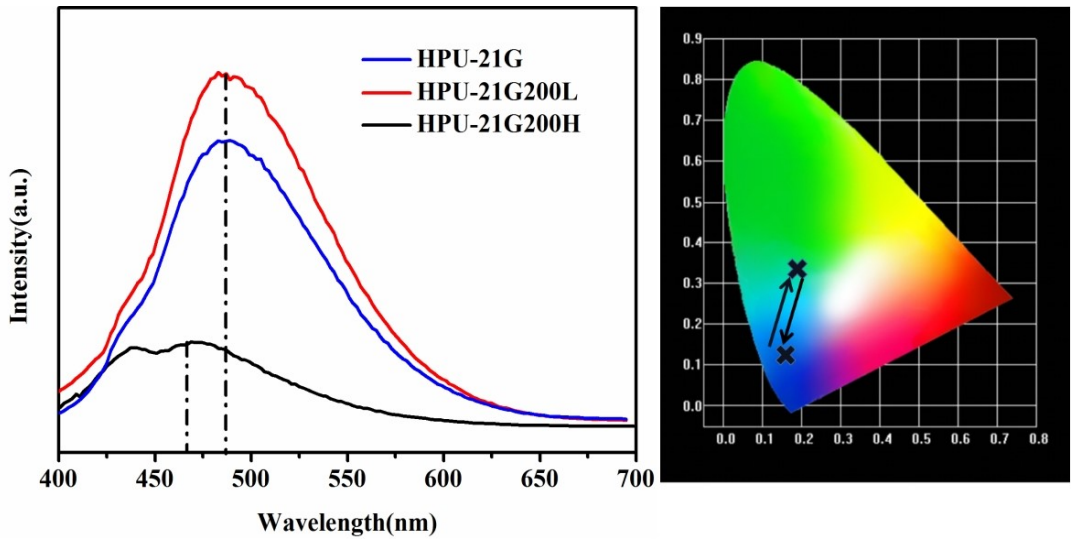

Figure S5. Emission spectra and CIE diagrams of **HPU-21G**, **HPU-21G200H** and **HPU-21G200L**.

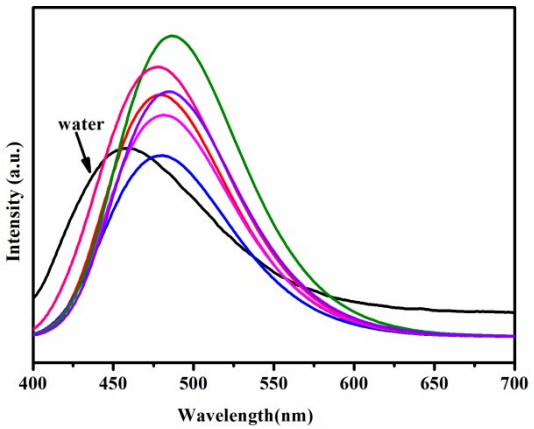

Figure S6. The fluorescence spectra of **HPU-21G** in different solvents.

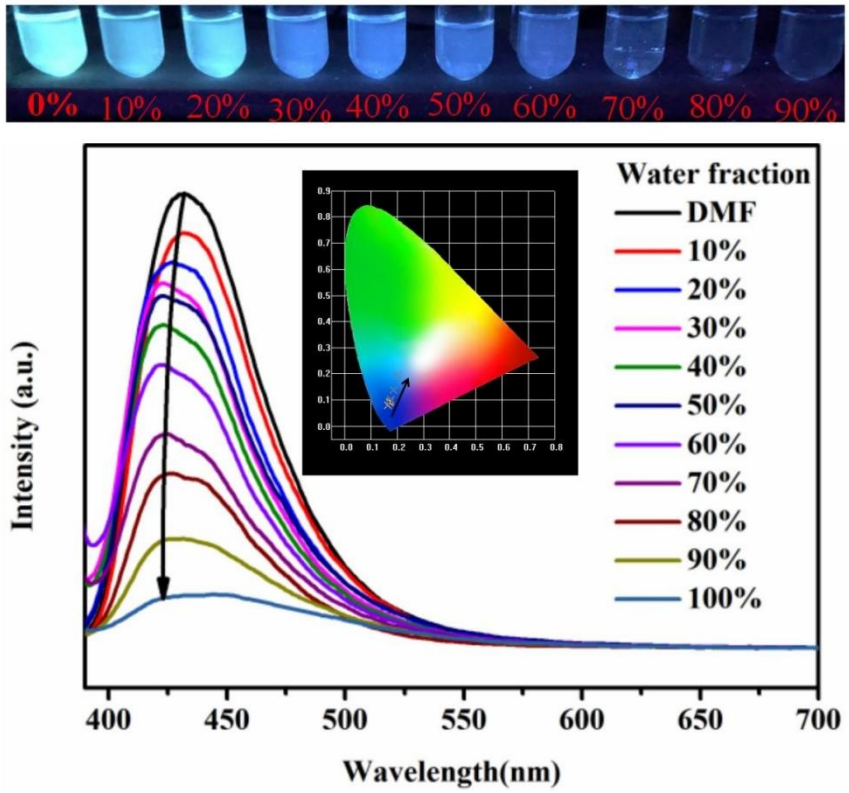

Figure S7. The fluorescence spectra of **HPU-21G** in DMF with different water contents (inset: the corresponding diagram of CIE change).

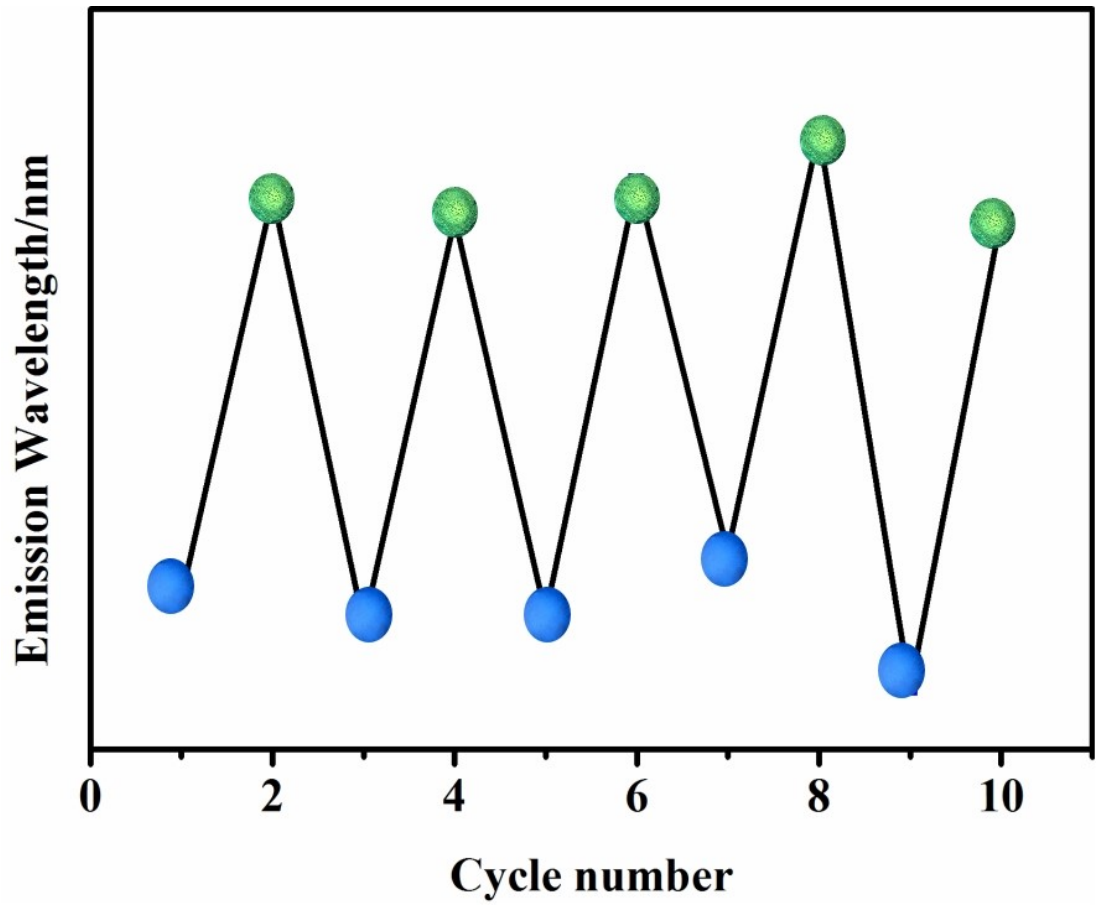

Figure S8. Reversible variation of the maximum emission intensity (437 and 496 nm) for **HPU-21G** under alternate treatment of wetting and air-drying in room temperature.

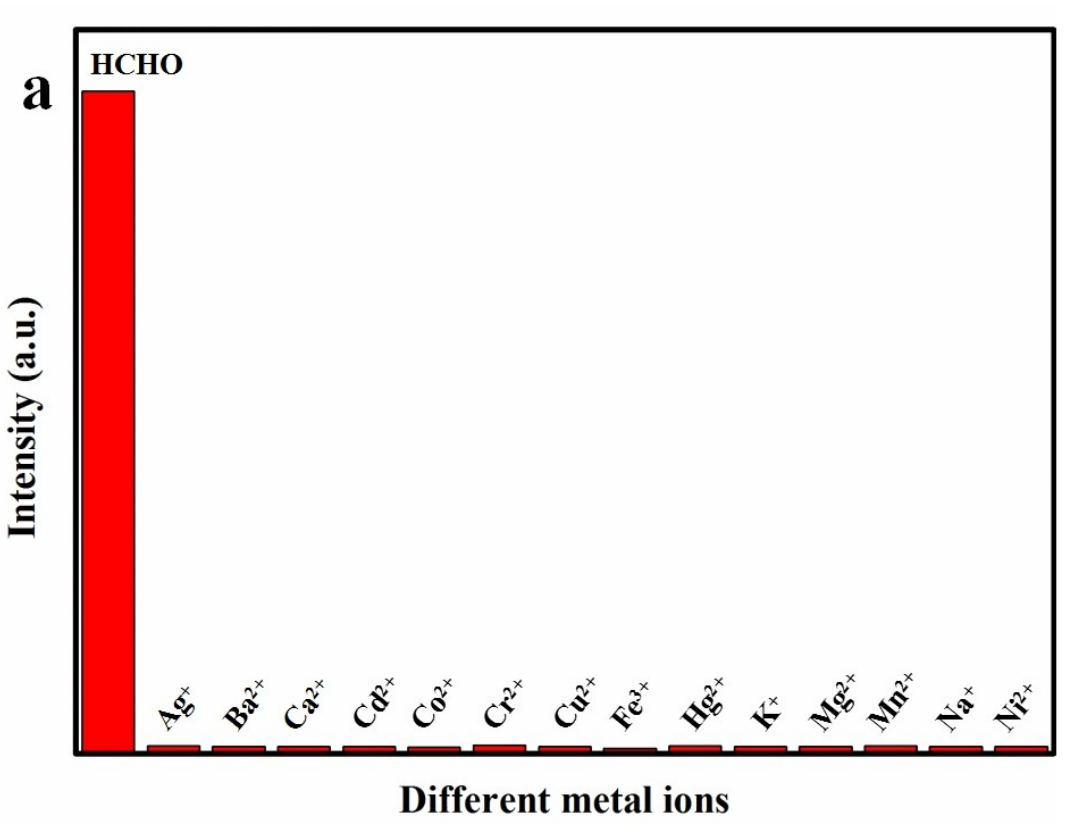
a
HCHO
Intensity (a.u.)
Ag+
Ba2+
Ca2+
Cd2+
Co2+
Cr2+
Cu2+
Fe3+
Hg2+
K+
Mg2+
Mn2+
Na+
Ni2+
Different metal ions

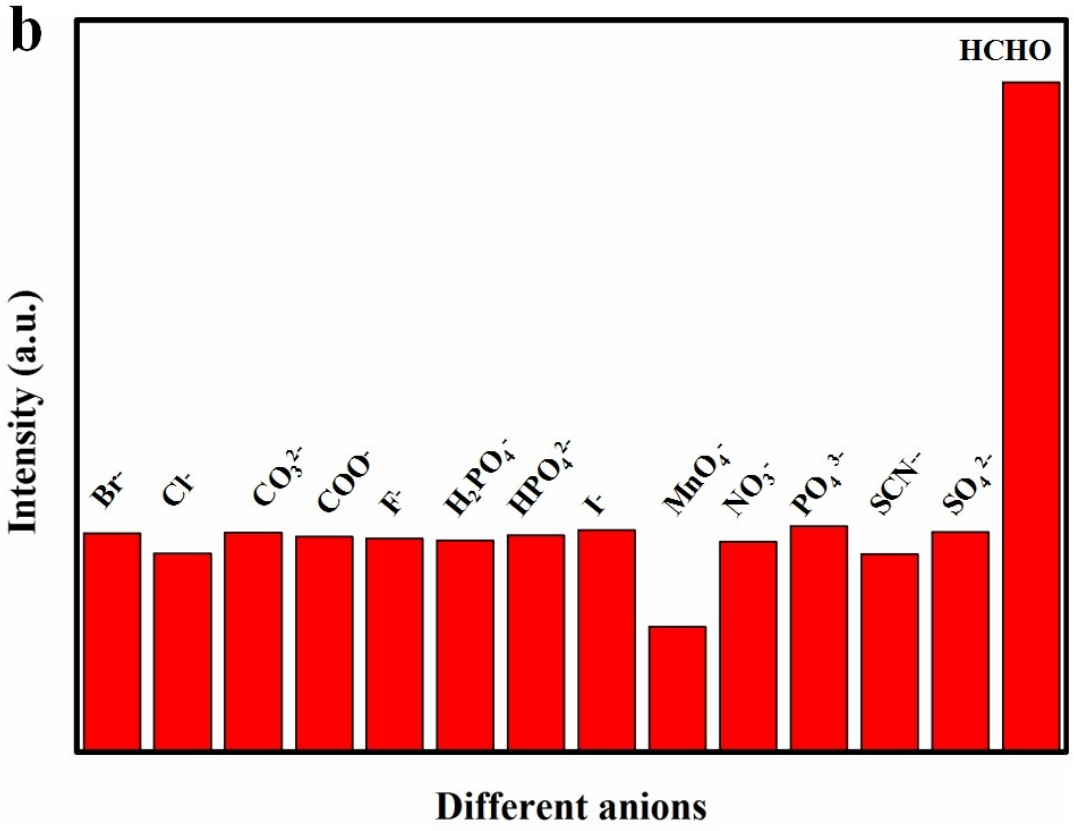
b
HCHO
Intensity (a.u.)
Br-
Cl-
CO3 2-
COO-
F-
H2PO4-
HPO4 2-
I-
MnO4-
NO3-
PO4 3-
SCN-
SO4 2-
Different anions

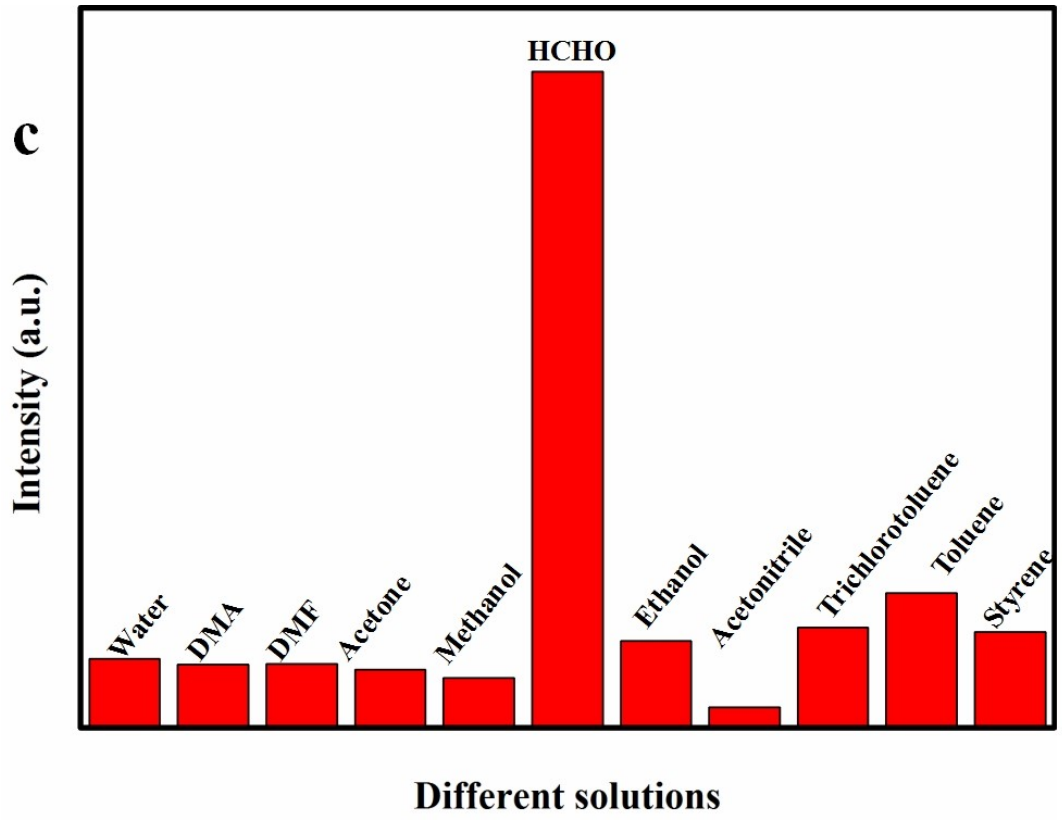

Figure S9. The comparision of the fluorescence intensity of the crystal suspension agent in different solvents and ions.

Table S2. Comparison of HCHO detection limits of different fluorescent probes.

Fluorescent materials	Detection limits (μM)	Ref.
Eu/Zr-MOF	0.2 ppm	1
$[(C_4H_9)_4N]_4H[PMo_{10}V_2O_{40}]$	0.2 ppm	2
Co_5-based MOF	10 ppm	3
MIL-101(Cr)	1.79 ppm	4
MPIPA	0.32μM	5

1 C. M. Li, J. P. Huang, H. L. Zhu, L. L. Liu, Y. M. Feng, G. Hu and X. B. Yu, *Sens. Actuators B: Chem.*, 2017, **253**, 275-282.

2 M. I. S. Veríssimo, J. A. F. Gamelas, A. J. S. Fernandes, D. V. Evtuguin and M. T. S. R. Gomes, *Food Chem.*, 2020, **318**, 126461.

3 W. Zhou, Y.-P. Wu, J. Zhao, W.-W. Dong, X.-Q. Qiao, D.-F. Hou, X. H. Bu and D.-S. Li, *Inorg. Chem.*, 2017, **56**, 14111-14117.

4 E. Haghighi and S. Zeinali, *Microporous Mesoporous Mater.*, 2020, **300**,

110065.

5 T. Gao, X. Cao, A. Bi, J. Dong, S. Huang, X. Huang, S. Wen and W. Zeng, *Sens. Actuators B: Chem.*, 2018, **273**, 1139-1145.